OPEN ACCESS
IOP Publishing
Superconductor Science and Technology
Supercond. Sci. Technol. **31** (2018) 045004 (8pp)
https://doi.org/10.1088/1361-6668/aaab81

Ballistic Josephson junctions based on CVD graphene

Tianyi Li[1,2,3], **John Gallop**[3], **Ling Hao**[3] and **Edward Romans**[1,2]

[1] London Centre for Nanotechnology, University College London, London WC1H 0AH, United Kingdom
[2] Department of Electronic and Electrical Engineering, University College London, London WC1E 6BT, United Kingdom
[3] National Physical Laboratory, Teddington TW11 0LW, United Kingdom

E-mail: tianyi.li.14@ucl.ac.uk and e.romans@ucl.ac.uk

Received 4 December 2017, revised 17 January 2018
Accepted for publication 30 January 2018
Published 22 February 2018

Abstract

Josephson junctions with graphene as the weak link between superconductors have been intensely studied in recent years, with respect to both fundamental physics and potential applications. However, most of the previous work was based on mechanically exfoliated graphene, which is not compatible with wafer-scale production. To overcome this limitation, we have used graphene grown by chemical vapour deposition (CVD) as the weak link of Josephson junctions. We demonstrate that very short, wide CVD-graphene-based Josephson junctions with Nb electrodes can work without any undesirable hysteresis in their electrical characteristics from 1.5 K down to a base temperature of 320 mK, and their gate-tuneable critical current shows an ideal Fraunhofer-like interference pattern in a perpendicular magnetic field. Furthermore, for our shortest junctions (50 nm in length), we find that the normal state resistance oscillates with the gate voltage, consistent with the junctions being in the ballistic regime, a feature not previously observed in CVD-graphene-based Josephson junctions.

Supplementary material for this article is available online

Keywords: Josephson junction, graphene, CVD, ballistic, SGS junction, hybrid structure

(Some figures may appear in colour only in the online journal)

1. Introduction

The experimental isolation of mono-layer graphene [1] has triggered an enormous effort to explore the new physical properties of graphene-superconductor hybrid structures. The unique band structure of graphene led to the prediction in 2006 that superconductor–graphene–superconductor (SGS) Josephson junctions should have a bipolar critical current that can be tuned from the electron band to the hole band by application of a gate voltage [2]. Such a unique property introduces a new degree of freedom for device operation, and offers the potential for a range of novel applications in magnetic metrology, quantum information, and other graphene-based electronics. Since the first SGS junction was experimentally realised by Heersche *et al* in 2007 [3], a number of papers on graphene- or thin-graphite-based Josephson junctions and superconducting quantum interference devices (SQUIDs) have been published [4–28], and many novel phenomena including multiple Andreev reflection [3, 4, 6–8, 14, 15, 18, 19, 21, 24] and ballistic transport [15, 17, 19–21, 24, 28] have been discovered and discussed. Operating devices with clean junctions in the ballistic regime could lead to performance improvements such as a lower intrinsic noise than for traditional tunnel junction-based devices [28]. The earliest work on SGS junctions was mainly based on mechanically exfoliated graphene [3–14, 16, 22, 23], due to the quality and easy availability of such samples. To reduce disorder, and allow exploration of new physics in the ballistic regime of SGS junctions, various

treatments to mechanically exfoliated graphene have been investigated such as suspending it [15, 24], or encapsulating it in exfoliated hexagonal boron nitride [17, 20, 21, 27, 28]. However, the fabrication and measurement of SGS junctions compatible with wafer-scale production remains largely unexplored, and circuits involving many SGS junctions are still a long way off. Recently, a few reports on SGS junctions based on epitaxial graphene on a SiC substrate [25] or graphene grown by chemical vapour deposition (CVD) [26] have been published, but in both cases the junctions were in the diffusive regime where the junction length was longer than the mean free path.

Here we report our study on much shorter SGS junctions based on CVD graphene. The fabrication process has been carefully optimised to be compatible with very short and wide junctions. We show that these junctions exhibit ideal *I*–*V* characteristics and an ideal Fraunhofer pattern in a perpendicular magnetic field, and that the junction critical current can be effectively tuned by the application of a gate voltage. Due to a higher density of scattering centres, CVD graphene typically has a shorter mean free path than exfoliated graphene, although mean free paths of up to 28 μm have recently been reported in fully encapsulated CVD graphene [29]. However, our carefully controlled fabrication technique allows us to build junctions as short as 50 nm, which is comparable or shorter than the mean free path in our unencapsulated samples. Consequently, we managed to observe the oscillation of the junction normal state resistance versus gate voltage in more than one device, indicating that our shortest junctions are in the ballistic regime. The ballistic transport is also consistent with the behaviour of the critical current as a function of temperature.

2. Methods

We have developed a robust process to fabricate Josephson junctions based on CVD graphene, which is compatible with mass production. The CVD graphene samples used in our experiment (Graphenea^{TM}) were synthesised and transferred to a silicon substrate with a 300 nm thick oxide layer. The as-transferred graphene was characterised by atomic force microscopy and Kelvin probe force microscopy, which showed that the silicon substrate was fully covered by graphene, mostly mono-layer (supplementary data is available online at stacks.iop.org/SUST/31/045004/mmedia). To fabricate the Josephson junctions, we used electron beam lithography (EBL) to define superconducting (Nb) electrodes on top of the graphene. After developing the e-beam resist, a tri-layer of Ti(5 nm)/Nb(70 nm)/Au(8 nm) was sputtered onto the sample, followed by lift-off without sonication. Ti was used here as an adhesive layer, while Au was sputtered immediately after Nb to prevent its oxidation. Since sputtered atoms are less directional than evaporated atoms, sputtering and lift-off are somewhat incompatible with each other in a normal micro-fabrication process, especially for small structures with dimensions of tens of nanometres. However, by using a double-layer of poly(methyl methacrylate) (PMMA) as the e-beam resist and sputtering the tri-layer at a lower rate to prevent overheating the sample, we managed to fabricate short and wide Josephson junctions with a very high throughput. We have inspected the fabrication of hundreds of devices in a single EBL process, and the visible yield is higher than 95%. After defining the junctions, another EBL process was used to remove the graphene surrounding the devices by Ar milling, so that the devices were isolated from one another and the junctions had no additional shunt resistance outside the gap region between the electrodes. The highly doped silicon substrate was connected as the back-gate electrode. A major concern in the fabrication was to reduce the junction normal state resistance R_n so as to increase the junction critical current I_c to an easy-to-measure level. Thus, we chose to fabricate junctions of short length L, in the range 50–850 nm, and large width, $W = 10$–80 μm, i.e. with an aspect ratio L/W from $\sim 1/100$ to $\sim 1/1600$ (figure 1). The contact resistance is also minimised by keeping the graphene free from polymer residue after the transfer to the silicon substrate, and also by depositing the junction electrodes in the first EBL process when the graphene surface is the cleanest. As shown in table S3 in the supplementary data, the average contact resistivity we obtain between graphene and the Nb electrode is $\sim 100\,\Omega\,\mu$m, which is amongst the lowest reported in the literature for grapheme/metal contacts [30–35]. Since each superconducting electrode induces a superconducting pair potential $\Delta(\mathbf{r})$ in the underlying graphene by the proximity effect, the resulting weak link is effectively two-dimensional with its normal region defined by the graphene between the electrodes [2].

3. Results and discussion

We measured the electronic properties of the graphene-based Josephson junctions using a normal 4-probe configuration, in a ^{3}He cryostat with a base temperature of 320 mK. As shown in figure 2(a), the junctions exhibit *I*–*V* characteristics at the base temperature without any hysteresis, as predicted by the resistively and capacitively shunted junction model for over-damped junctions with a Stewart–McCumber parameter, $\beta_c = 2\pi I_c R_n{}^2 C/\Phi_0 < 1$. For the 250 nm long, 80 μm wide junction shown, the normal state resistance, $R_n \sim 5\ \Omega$, and we estimate the capacitance of the junction (coupled via the back-gate) is $C \sim 2 \times 10^{-14}$ F so that $\beta_c \sim 0.02$, indicating that the junctions are non-hysteretic, which is important for the standard operation and readout of many devices based on Josephson junctions such as the dc SQUID. As temperature gradually increases, the critical current I_c becomes smaller, and the transition close to I_c becomes slightly rounded, which is expected for a strongly over-damped junction with increasing thermal noise. For junctions shorter than 250 nm, the Josephson effect is still obvious up to a critical temperature T_c around 1.5 K, indicating that such junctions can operate over a usefully wide temperature range. By plotting the differential resistance dV/dI as a function of bias current (figure 2(b)), we can see the trend more clearly. The two peaks in the dV/dI curves, indicating the transition at $\pm I_c$,

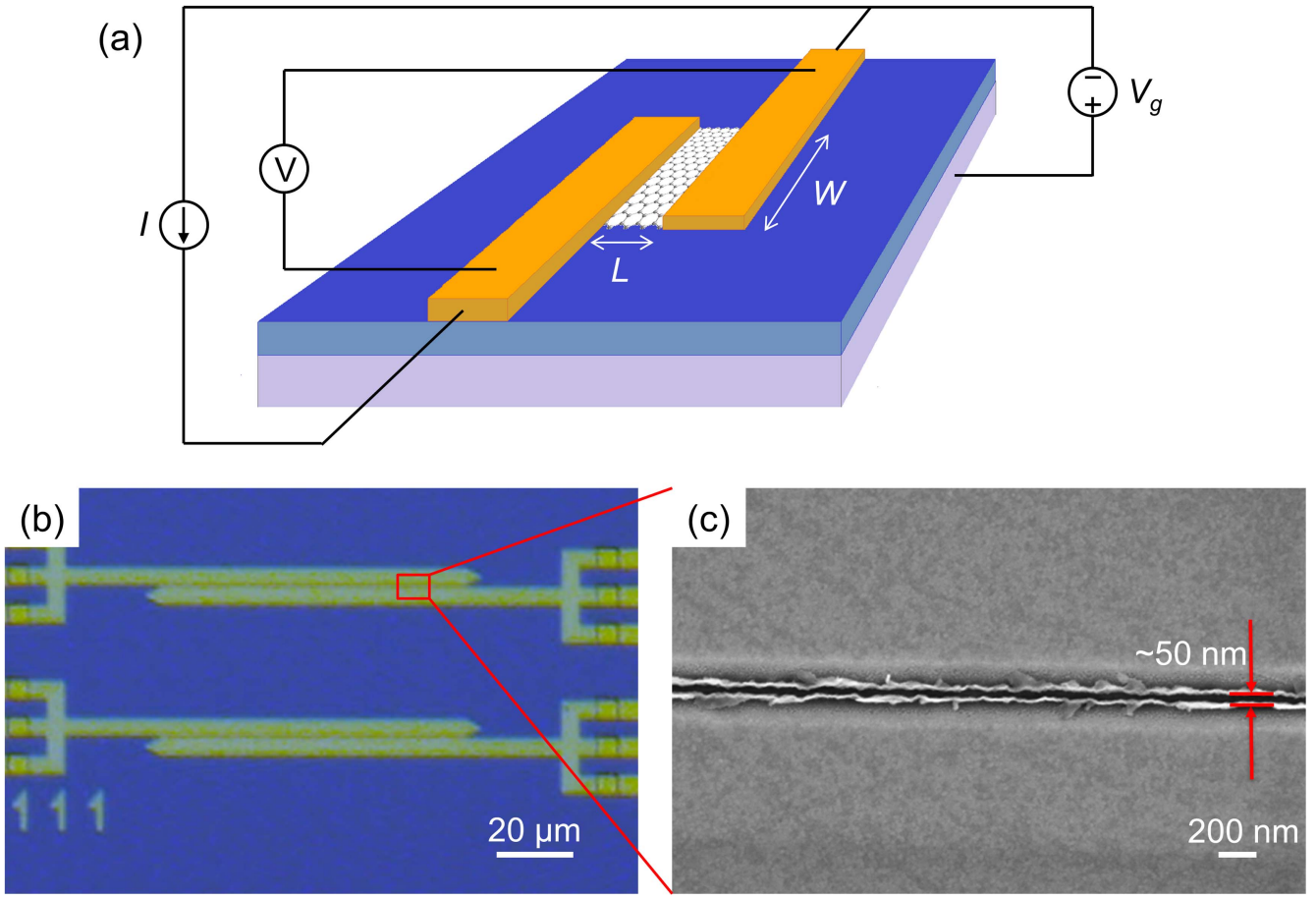

Figure 1. (a) Schematic diagram (not to scale) of a superconductor–graphene–superconductor (SGS) Josephson junction fabricated on a silicon substrate with an oxide layer. The junction is of length L and width $W \gg L$. The connections used for four-probe I–V measurements with an applied gate voltage V_g are also shown. (b) Optical microscope image showing two 80 μm wide Josephson junctions fabricated using CVD graphene with Ti/Nb/Au electrodes. (c) SEM image of part of one junction, marked by the red box in (b), showing that the junction is only 50 nm in length.

gradually become weaker in height and closer to each other as the temperature increases.

To investigate this further, we plot the critical current as a function of temperature for junctions with lengths from 50 to 450 nm, in figures 2(c)–(f) respectively. For each device, the critical current I_c increases as the temperature T decreases. However, the I_c–T curves are not identical in shape. For the 150 nm and 250 nm long junctions, the critical current I_c tends to saturate when $T \lesssim T_c/3$ whereas for the 50 nm long junction, the critical current I_c is still increasing at the lowest temperatures. For the 450 nm long junction, the critical current I_c also tends to saturate, however, as its T_c is smaller than that of the other junctions, the saturation is not quite fully realised at the lowest temperature we can reach. Such a difference in the I_c–T curves can be well explained by the theory of a weak link in either the 'dirty' or 'clean' limit developed by Kulik and Omelyanchuk (the KO-1 and KO-2 theories) [36, 37]. A weak-link junction is in the dirty limit if the junction length L is much longer than the mean free path l, and is in the clean limit if $L < l$. For a weak-link junction in the dirty limit, KO-1 theory predicts the supercurrent I_s is related to temperature T by

$$I_s(T, \varphi) = \frac{2\pi k_B T}{eR_n} \times \sum_{\omega>0} \frac{2\Delta \cos(\phi/2)}{\delta} \arctan \frac{\Delta \sin(\varphi/2)}{\delta}, \quad (1)$$

where R_n is the normal state resistance of the junction, $\Delta = \Delta(T)$ is the temperature-dependent energy gap of the superconductor, $\omega = \pi k_B T(2n + 1)/\hbar$ is the Matsubara frequency for integer n, φ is the phase difference across the weak link, and $\delta = \sqrt{\Delta^2 \cos^2(\varphi/2) + (\hbar\omega)^2}$. For a weak link in the clean limit, the I_s–T relationship is described by the KO-2 theory as

$$I_s(T, \varphi) = \frac{\pi\Delta}{eR_n} \sin(\varphi/2) \tanh \frac{\Delta \cos(\varphi/2)}{2k_B T}. \quad (2)$$

The respective expressions in (1) and (2) have been shown by Beenakker [38] to agree with his more general analysis of point contact weak links in the disordered regime (for $T \to 0$) and ballistic regime (for all T in the classical limit). For a given T, (1) and (2) need to be maximised over φ to determine $I_c(T)$. We assume that $\Delta(T)$ follows the usual

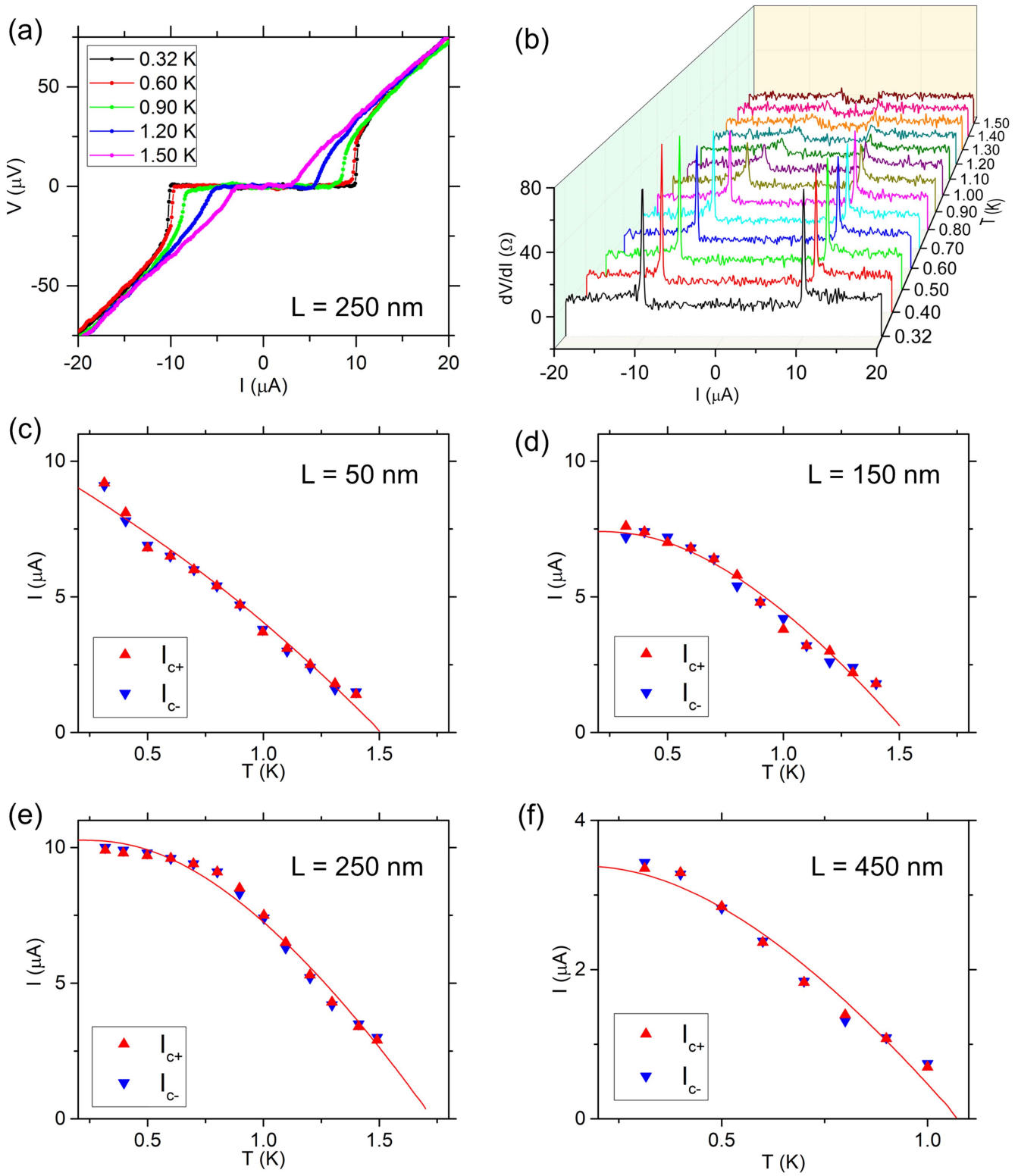

Figure 2. *I*–*V* characteristics of the junctions versus temperature. (a) *I*–*V* characteristics of a 250 nm long SGS junction measured at different temperatures. (b) The differential resistance dV/dI versus bias current I, measured on this 250 nm long SGS junction from 0.32 to 1.50 K. (c)–(f) The critical current I_c versus temperature T, measured on (c) 50 nm long, (d) 150 nm long, (e) 250 nm long, and (f) 450 nm long SGS junctions, respectively. The red curve in (c) is the fitting of I_{c+} (from the positive *I*–*V* branch) by KO-2 theory, while the red curves in (d)–(f) are the fitting of I_{c+} by KO-1 theory, as described in the main text. All the junctions are 80 μm wide.

form of the Bardeen–Cooper–Schrieffer theory [39] in the weak-coupling limit where $\Delta(0) = 1.764 k_B T_c$ and $\Delta(T)/\Delta(0)$ is a function of T/T_c. Qualitatively the I_c–T curves predicted by the KO-1 and KO-2 theory almost coincide with each other when the temperature is close to T_c, but as temperature decreases, the I_c of a dirty junction tends to saturate while the I_c of a clean junction is still increasing [40]. As shown by the red curves in figures 2(c)–(f), the measured I_c–T curves of the junctions longer than 150 nm can be well fitted by the KO-1 theory, while the I_c–T curve of the 50 nm long junction is better fitted by the KO-2 theory. (In the fitting we add an adjustable pre-factor α to the right-hand side of (1) and (2) to represent the depression of the I_cR_n product found in real devices as discussed below. Detailed fitting results are given in the supplementary data.) This suggests that junctions longer than 150 nm are in the dirty regime where the transport of charge carriers in the graphene is diffusive, while the 50 nm long junction is in the clean regime where ballistic transport takes place in the graphene. According to the fits, the junction transition temperature T_c is 1.06–1.73 K, which is smaller than that of the superconducting electrodes ($T_c \sim 9$ K). This is probably because the interface between the graphene and the superconducting electrode is not highly transparent, so that the superconducting pairing induced in the graphene by the proximity effect is weakened. Similar behaviour has been seen in other SGS junctions [8]. The critical current also shows reasonable dependence on junction length. As we can see in figure 2(f), the critical current I_c of the 450 nm long junction is much smaller than others. We also fabricated and measured an 850 nm long junction which shows no Josephson effect at all. This allows us to estimate the normal state coherence length in graphene, $\xi_{N,}$ to be of several hundred nanometres. For the three shorter junctions, the critical current I_c at the base temperature does not show a strong dependence on the junction length. This is because the contact resistance between the graphene and the superconducting electrode, which has some device-to-device variation, makes a large contribution to the measured normal state resistance R_n, as will be verified below. This leads to some device-to-device variation in I_c since it is inversely proportional to R_n in both the KO-1 and KO-2 theories, and masks any dependency on the junction length for the shorter devices.

We also measured the electronic properties of the junctions in a perpendicular magnetic field. As Josephson junctions with finite area, they are expected to show the effect of quantum interference, since the perpendicular magnetic field can induce a phase difference between the supercurrent at different points across the junction width. In figure 3, we plot dV/dI as a function of bias current I and magnetic field B in a 2D colour scale plot for a 250 nm long, 80 μm wide junction. The purple region is where the differential resistance is zero, and the outline of this region indicates the critical current. As can be seen in the plot, the outline of the purple region can be perfectly fitted by an ideal Fraunhofer-like pattern, $I_c \propto \sin(\pi B/\Delta B)/(B/\Delta B)$, as indicated by the black dashed lines, where ΔB is the field needed to reach the first minimum. The higher-order peaks, though not as high in contrast as the central ones, are still clearly visible. In a wider field sweep on the same device, we managed to see peaks up to $\pm 80\ \mu$T (supplementary figure S3). The observation of the Fraunhofer pattern indicates that the junction, although having an aspect ratio of $L/W = 1/320$, is still quite uniform in terms of the distribution of its supercurrent density. Since the first minimum corresponds to one flux quantum Φ_0 in the junction, we can calculate the measured effective area of the junction as $A_{eff} = \Phi_0/\Delta B = 280\ \mu m^2$. This is much larger than the simple theoretical estimate of $A_{theo} = (L + 2\lambda)W = 26\ \mu m^2$, corresponding to the area of the normal region plus the area of each electrode the field penetrates into over a distance of order the superconducting penetration depth, λ (which is approximately 37.5 nm for Nb). However, this estimate of A_{theo} ignores the strong flux focusing in the junction caused by the Meissner effect in the electrodes. Each electrode extends 5 μm away from the normal region and thus has a much larger area. The measured value A_{eff} corresponds to about 35% of the flux applied to each electrode being forced into the normal region, so this is a reasonable explanation for the discrepancy between A_{eff} and A_{theo}.

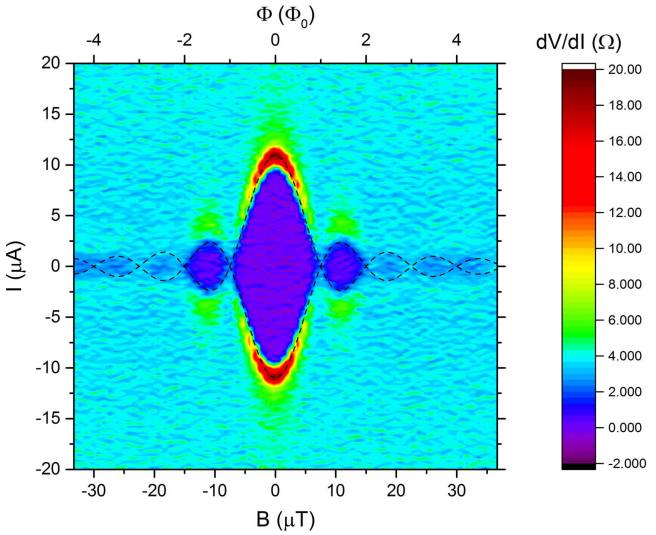

Figure 3. *I–V* characteristics under a perpendicular magnetic field. The differential resistance dV/dI is plotted as a function of bias current I and magnetic field B, measured on a 250 nm long, 80 μm wide SGS junction at 320 mK, showing an ideal Fraunhofer-like interference pattern. The shape of the pattern can be well fitted by $I_c \propto \sin(\pi B/\Delta B)/(B/\Delta B)$, as indicated by the black dashed lines, where ΔB is the field need to reach the first minimum.

One of the key advantages of a graphene-based Josephson junction is that the critical current can be easily tuned by the gate voltage, V_g, thanks to the relatively low density of states in graphene [3–6, 8–15, 18, 20–23, 26]. In figure 4(a) we show *I–V* curves measured on a 50 nm long, 10 μm wide junction under different gate voltages. Unlike the dependence on temperature, the gate voltage not only affects the critical current, but also the normal state resistance. The effect is more clearly demonstrated if we plot dV/dI as a function of bias current and gate voltage in a 2D colour plot (figure 4(b)). As the gate voltage increases from -50 V to $+90$ V, the critical current (the boundary of the dark blue region)

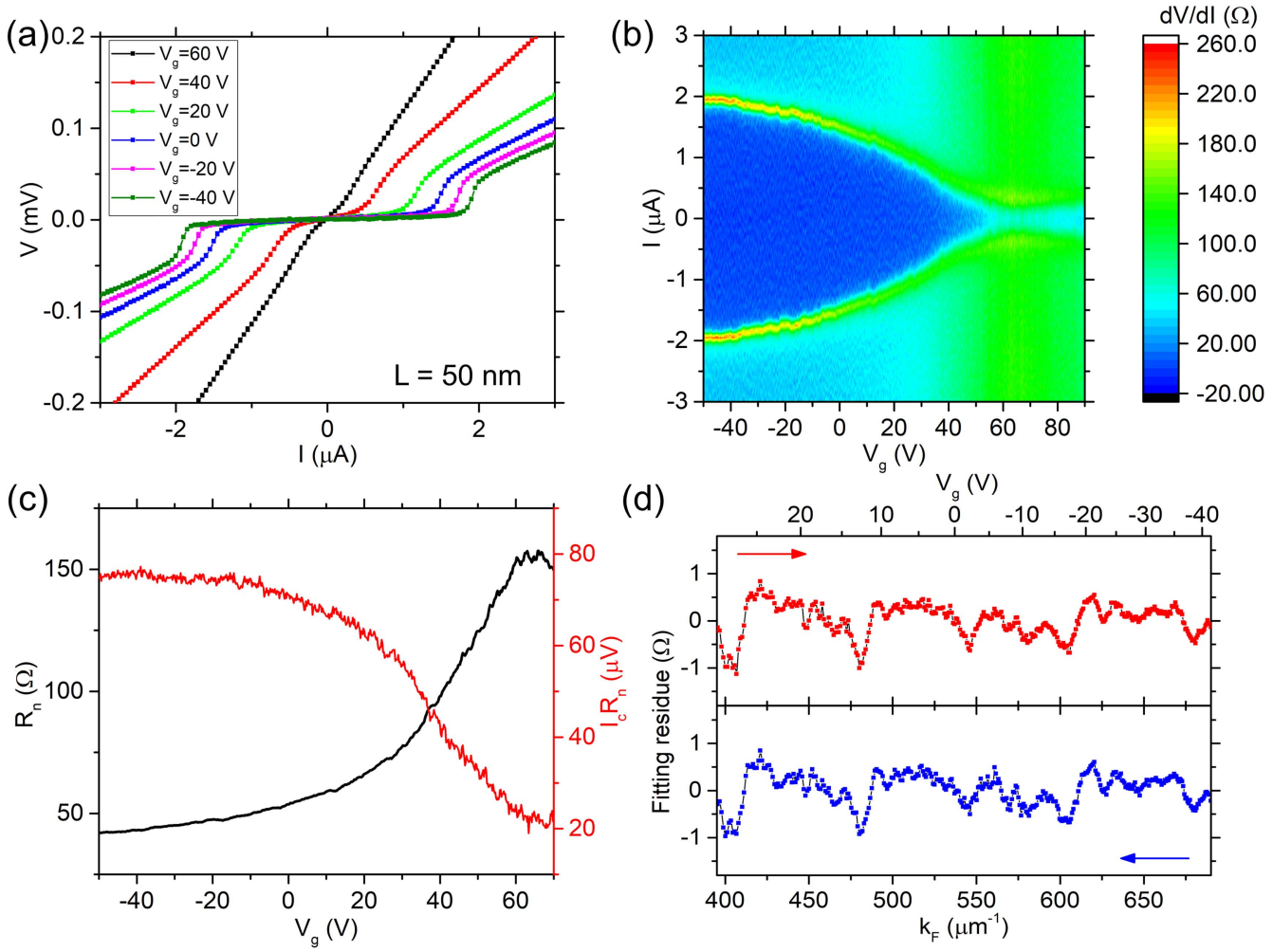

Figure 4. Electronic properties of a 50 nm long, 10 μm wide SGS junction versus gate voltage. (a) I–V characteristics of the junction under different gate voltages. (b) Colour scale plot of the differential resistance $\mathrm{d}V/\mathrm{d}I$ as a function of bias current I and gate voltage V_g. (c) Normal state resistance R_n and the product $I_\mathrm{c}R_\mathrm{n}$ versus gate voltage V_g. (d) The fitting residue versus either V_g or the equivalent Fermi wavenumber k_F (which is proportional to $\sqrt{|V_\mathrm{g} - V_0|}$), after the R_n–$k_\mathrm{F}(V_\mathrm{g})$ curve is fitted by a smooth polynomial. The red points are for k_F swept upwards (V_g swept downwards); the blue points are for k_F swept downward (V_g swept upwards). The two sweep directions show similar periodic oscillations. All data was measured at 320 mK.

gradually decreases from 1.8 μA, reaches the minimum of 0.14 μA at the Dirac point (where $V_\mathrm{g} = V_0 = 63.85$ V), and then starts to increase. The critical current can be effectively tuned by an order of magnitude by the gate voltage, allowing more flexibility in the operation of Josephson junctions.

The product of critical current I_c and normal state resistance R_n is the characteristic switching voltage when the junction jumps from the superconducting state to the normal state around the critical current. For a short ideal SGS junction in either the dirty or the clean limit, the product $I_\mathrm{c}R_\mathrm{n}$ is a figure of particular interest since it is solely determined by the operating temperature and the energy gap of the superconductor, and should be independent of the gate voltage, as indicated by the form of (1) and (2). In figure 4(c) we plot both the normal state resistance R_n and the product $I_\mathrm{c}R_\mathrm{n}$ as a function of the gate voltage, for a 50 nm long junction. As the gate voltage draws closer to the Dirac point, the critical current decreases while the normal state resistance increases. Their product $I_\mathrm{c}R_\mathrm{n}$ remains constant when the gate voltage is far away from the Dirac point; however, it drops as the gate voltage approaches the Dirac point. Even in the constant regime, the measured value of $I_\mathrm{c}R_\mathrm{n}$ is only $\sim 1/6$ of the theoretical one determined by (2). Such suppression of $I_\mathrm{c}R_\mathrm{n}$ is frequently discussed in previous reports on graphene-based Josephson junctions, and there still remains some controversy about the exact cause. Many authors believe that the overall suppression of $I_\mathrm{c}R_\mathrm{n}$ is a result of the likely imperfect interface between graphene and the superconductor [13, 15, 18, 26] as mentioned above. As to the further drop of $I_\mathrm{c}R_\mathrm{n}$ near the Dirac point, most authors believe that it is caused by a discrepancy between the intrinsic critical current and the measured critical current due to premature switching, which is expected to be more pronounced near the Dirac point [3, 4, 6, 8]. However, others attribute the suppression of $I_\mathrm{c}R_\mathrm{n}$ to specular Andreev reflection that occurs close to the Dirac point [13].

Small oscillations can be seen over a wide range of gate voltages in the R_n–V_g curve in figure 4(c), the physical origin of which is worth investigating. These may be caused by

universal conductance fluctuations in the graphene; or they may instead be due to the phase-coherent interference of charge carriers in the Fabry–Perot cavity defined by the n–p–n junction that arises from the different doping levels in the exposed graphene (in the normal region of the junction) and the non-exposed graphene (under the electrodes). If the oscillation is dominated by universal conductance fluctuations, the oscillation will be reproducible but random without any periodicity. However, for the Fabry–Perot mechanism we would expect to see a local minimum whenever an integer multiple of the Fermi wavelength $k_F(V_g)$ of the charge carriers is equal to the effective length of the n–p–n junction. To investigate the mechanism of the oscillation, we plot the normal state resistance R_n versus the Fermi wavenumber $k_F = \sqrt{2\pi C_{ox}|V_g - V_0|/e}$, where C_{ox} is the area capacitance between the gate electrode and graphene, and then fit the R_n–$k_F(V_g)$ curve by a smooth polynomial. We can see the oscillation more clearly in the fitting residues, as shown in figure 4(d). The upper and lower panels of figure 4(d) display the fitting residues when k_F is swept upwards and downwards respectively, which shows that the oscillation is highly reproducible. For both curves, beyond the small amplitude fluctuations, there exist periodic minima with an even spacing of $\Delta k_F \sim 75\ \mu m^{-1}$. If such periodic minima result from the phase-coherent interference of charge carriers in the Fabry–Perot cavity defined by the n–p–n junction, this implies the effective length of the junction is $2\pi/\Delta k_F \sim 83$ nm, which is quite reasonable considering the geometric length. Such periodic oscillation thus provides more compelling evidence that the junction is in the ballistic regime. Similar oscillations were observed in a series of 50 nm long junctions with different widths (the narrower the junction, the higher the oscillation amplitude), but not in any junctions longer than 150 nm. This suggests that the shortest junctions are ballistic while the longer ones are diffusive, allowing us to estimate the mean free path in the graphene to be between 50 and 150 nm. The mean free path l in graphene can also be precisely calculated by fitting the R_n–V_g curve to a model [41] in which the normal state resistance is a sum of the contact resistance and the resistance of graphene between the electrodes. This gives

$$R_n = 2R_c + \frac{L/W}{e\mu\sqrt{n_i^2 + \left[\frac{C_{ox}}{e}(V_g - V_0)\right]^2}}, \qquad (3)$$

where R_c is the contact resistance between the graphene and each electrode, μ is the mobility of charge carriers in graphene and n_i is the area carrier density of graphene caused by impurities. After fitting the R_n–V_g curve of the 850 nm long device, we obtain the conductivity of the graphene, $\sigma = e\mu\sqrt{n_i^2 + \left[\frac{C_{ox}}{e}(V_g - V_0)\right]^2} = 2.2$ mS, and the area carrier density of graphene, $n = \sqrt{n_i^2 + \left[\frac{C_{ox}}{e}(V_g - V_0)\right]^2} = 4.9 \times 10^{12}\ cm^{-2}$ (see supplementary data for detailed fitting results). Thus, the mean free path can be calculated as $l = \sigma h/2e^2\sqrt{n\pi} = 72$ nm, which is in excellent agreement with our estimated range above. The validity of these parameters was further confirmed by measurements on a separate Hall bar structure fabricated on the same wafer (see supplementary data). The fitting of the R_n–V_g curve above also verifies that the contact resistance between the graphene and the superconducting electrodes accounts for a large proportion of the normal state resistance.

4. Conclusion

In conclusion, we have developed a reliable method to fabricate Nb/graphene/Nb Josephson junctions based on CVD graphene, which is important for both fundamental research and applications. The excellent quality of our junctions has been demonstrated by a series of measurements. The junctions can work over a wide temperature range from at least 320 mK to 1.50 K without any hysteresis, and exhibit an ideal Fraunhofer quantum interference pattern in a perpendicular magnetic field, showing the uniform distribution of the supercurrent in the junction. By carefully optimising the fabrication process, we have managed to reduce the junction length to 50 nm, shorter than the mean free path, so that evidence of ballistic transport can be observed. As far as we know, this is the first time that ballistic transport has been observed in a Josephson junction based on CVD graphene. In addition, the critical current can be effectively modulated by the gate voltage, allowing more flexibility for device operation, such as gate-voltage-based control of flux or phase qubits incorporating Josephson junctions. The controllability of the critical current could also be particularly useful in applications involving arrays of Josephson junctions, such as dc SQUIDs and single flux quantum devices, where some junctions should ideally be identical, which cannot be achieved in practice due to limitations in fabrication. Thanks to the relatively low cost and high quality of CVD graphene, our device is compatible with large-scale production whilst maintaining its excellent properties, and so provides a competitive solution for superconducting electronics.

Acknowledgments

The authors thank A Zurutuza at Graphenea™ for the graphene samples, J Fenton for help with the low-temperature system, and P Warburton for comments on the manuscript. The work was funded by the UK National Measurement System (NMS) awards 119616 and 119610, and by the UK Engineering and Physical Sciences Research Council (EPSRC) awards EP/M508330/1, EP/J007137/1 and 1437148.

ORCID iDs

Tianyi Li https://orcid.org/0000-0001-7778-4825

References

[1] Novoselov K S, Geim A K, Morozov S V, Jiang D, Zhang Y, Dubonos S V, Grigorieva I V and Firsov A A 2004 *Science* **306** 666–9
[2] Titov M and Beenakker C W J 2006 *Phys. Rev.* B **74** 041401
[3] Heersche H B, Jarillo-Herrero P, Oostinga J B, Vandersypen L M K and Morpurgo A F 2007 *Nature* **446** 56–9
[4] Du X, Skachko I and Andrei E Y 2008 *Phys. Rev.* B **77** 184507
[5] Girit C, Bouchiat V, Naamanth O, Zhang Y, Crommie M F, Zetti A and Siddiqi I 2009 *Nano Lett.* **9** 198–9
[6] Miao F, Bao W Z, Zhang H and Lau C N 2009 *Solid State Commun.* **149** 1046–9
[7] Ojeda-Aristizabal C, Ferrier M, Guéron S and Bouchiat H 2009 *Phys. Rev.* B **79** 165436
[8] Jeong D, Choi J H, Lee G H, Jo S, Doh Y J and Lee H J 2011 *Phys. Rev.* B **83** 094503
[9] Lee G H, Jeong D, Choi J H, Doh Y J and Lee H J 2011 *Phys. Rev. Lett.* **107** 146605
[10] Borzenets I V, Coskun U C, Jones S J and Finkelstein G 2011 *Phys. Rev. Lett.* **107** 137005
[11] Coskun U C, Brenner M, Hymel T, Vakaryuk V, Levchenko A and Bezryadin A 2012 *Phys. Rev. Lett.* **108** 097003
[12] Popinciuc M, Calado V E, Liu X L, Akhmerov A R, Klapwijk T M and Vandersypen L M K 2012 *Phys. Rev.* B **85** 205404
[13] Komatsu K, Li C, Autier-Laurent S, Bouchiat H and Gueron S 2012 *Phys. Rev.* B **86** 115412
[14] Choi J H, Lee G H, Park S H, Jeong D C, Lee J O, Sim H S, Doh Y J and Lee H J 2013 *Nat. Commun.* **4** 2525
[15] Mizuno N, Nielsen B and Du X 2013 *Nat. Commun.* **4** 2716
[16] Borzenets I V, Coskun U C, Mebrahtu H T, Bomze Y V, Smirnov A I and Finkelstein G 2013 *Phys. Rev. Lett.* **111** 027001
[17] Calado V E, Goswami S, Nanda G, Diez M, Akhmerov A R, Watanabe K, Taniguchi T, Klapwijk T M and Vandersypen L M K 2015 *Nat. Nanotechnol.* **10** 761–5
[18] Li C, Guéron S, Chepelianskii A and Bouchiat H 2016 *Phys. Rev.* B **94** 115405
[19] Lee G, Kim S, Jhi S and Lee H 2015 *Nat. Commun.* **6** 7181
[20] Shalom M *et al* 2016 *Nat. Phys.* **12** 318–22
[21] Borzenets I V *et al* 2016 *Phys. Rev. Lett.* **117** 237002
[22] Tsumura K, Furukawa N, Ito H, Watanabe E, Tsuya D and Takayanagi H 2016 *Appl. Phys. Lett.* **108** 003109
[23] English C D, Hamilton D R, Chialvo C, Moraru I C, Mason N and Van Harlingen D J 2016 *Phys. Rev.* B **94** 115435
[24] Kumaravadivel P and Du X 2016 *Sci. Rep.* **6** 24274
[25] Jouault B *et al* 2016 *J. Supercond. Nov. Magn.* **29** 1145–50
[26] Ke C T *et al* 2016 *Nano Lett.* **16** 4788–91
[27] Nanda G, Aguilera-Servin J L, Rakyta P, Kormányos A, Kleiner R, Koelle D, Watanabe K, Taniguchi T, Vandersypen L M K and Goswami S 2017 *Nano Lett.* **17** 3396–401
[28] Thompson M D, Ben Shalom M, Geim A K, Matthews A J, White J, Melhem Z, Pashkin Y A, Haley R P and Prance J R 2017 *Appl. Phys. Lett.* **110** 162602
[29] Banszerus L, Schmitz M, Engels S, Goldsche M, Watanabe K, Taniguchi T, Beschoten B and Stampfer C 2016 *Nano Lett.* **16** 1387–91
[30] Xia F, Perebeinos V, Lin Y, Wu Y and Avouris P 2011 *Nat. Nanotechnol.* **6** 179–84
[31] Hsu A, Wang H, Kim K K, Kong J and Palacios T 2011 *IEEE Electron Device Lett.* **32** 1008–10
[32] Moon J S *et al* 2012 *Appl. Phys. Lett.* **100** 203512
[33] Li W *et al* 2013 *Appl. Phys. Lett.* **102** 183110
[34] Smith J T, Franklin A D, Farmer D B and Dimitrakopoulos C D 2013 *ACS Nano* **7** 3661–7
[35] Leong W S, Gong H and Thong J T L 2014 *ACS Nano* **8** 994–1001
[36] Kulik I O and Omelyanchuk A N 1975 *JETP Lett.* **21** 96–7
[37] Kulik I O and Omelyanchuk A N 1977 *Sov. J. Low Temp. Phys.* **3** 459–61
[38] Beenakker C W J 1992 *Transport Phenomena in Mesoscopic System* ed H Fukuyama and T Ando (Berlin: Springer) p 235
[39] Bardeen J, Cooper L N and Schrieffer J R 1957 *Phys. Rev.* **106** 1175–204
[40] Likharev K K 1979 *Rev. Mod. Phys.* **51** 101–59
[41] Kim S, Nah J, Jo I, Shahrjerdi D, Colombo L, Yao Z, Tutuc E and Banerjee S K 2009 *Appl. Phys. Lett.* **94** 062107